Journal of the Physical Society of Japan
Vol. 70, No. 2, February, 2001, pp. 481-491

Effective Mass Theory of Carbon Nanotubes with Vacancies in Magnetic Fields

Masatsura IGAMI, Takeshi NAKANISHI[1] and Tsuneya ANDO[2]

Institute of Materials Science, University of Tsukuba
1-1-1 Tennodai, Tsukuba, Ibaraki 305-8573
[1]*Department of Applied Physics and DIMES, Delft University of Technology*
Lorentzweg 1, 2628 CJ Delft, The Netherlands
[2]*Institute for Solid State Physics, University of Tokyo*
5-1-5 Kashiwanoha, Kashiwa, Chiba 277-8581

(Received June 29, 2000)

An effective-mass theory is developed on transport of non-doped carbon nanotubes with local and short-range impurities in the presence of a magnetic field. The conductance is shown to be scaled completely by the field component in the direction of impurities. In a weak-field regime, the conductance strongly depends on strength of potential and the difference in the number of impurities at A and B sublattices ΔN_{AB}. In a strong-field limit, the conductance is reduced to $e^2/\pi\hbar$ if impurities exist only on A or B sublattices and vanishes in all other cases. These results are intuitively understood by localized charge distribution of the wave function in magnetic fields.

KEYWORDS: carbon nanotube, conductance, effective-mass theory, magnetic field, impurity potential

§1. Introduction

Carbon nanotubes (CN's) are quasi one-dimensional materials which are built by wrapping a graphene sheet into tubes on nanometer scale.[1)] Electronic structure of a single CN has been studied theoretically, which predicted that CN becomes either metallic or semiconducting depending on its chiral vector, i.e., boundary conditions in the circumference direction.[2-11)] These predictions have been confirmed by Raman experiments[12)] and direct measurements of local density of states by scanning tunneling spectroscopy (STS).[13-15)] In view of mesoscopic physics, CN's are classified into a new kind of quantum wires which have unique geometric and electronic structures different from conventional ones fabricated using semiconductor heterostructures. The purpose of this work is to study effects of short-range impurities on transport of CN's in magnetic fields based on an effective-mass theory.

It is well known that defects play important roles in electronic states of CN's and graphene sheets. Effects of topological defects, i.e., five- or seven-member rings, in nanotube junctions were calculated and a universal power-law dependence on the conductance was shown.[16-18)] Electronic structure of CN's with various caps was also studied.[19)] In a graphene sheet with a finite width, localized edge states are formed near the Fermi level when the boundary is in a certain specific direction.[20-22)] In an effective-mass scheme, these defects can often be obtained by local boundary conditions imposed on envelope functions. For example, such edge states are easily obtained by imposing rigid boundary conditions along a line in a certain direction.

A point defect also leads to peculiar electronic states. STM images of a graphene sheet, simulated in the presence of a local point defect, showed that a $\sqrt{3}\times\sqrt{3}$ interference pattern is formed in the wave function near the impurity.[23)] This is intuitively understood by a mixing of wave functions at K and K' points.

Effects of scattering on impurity potential in CN's were studied theoretically and it was proved that a Born series for back-scattering vanishes identically for scatterers having a potential with a range larger than the lattice constant.[24, 25)] This intriguing fact was related to Berry's phase acquired by a rotation in the wave-vector space in the system described by a $\boldsymbol{k}\cdot\boldsymbol{p}$ Hamiltonian.[26)]

The $\boldsymbol{k}\cdot\boldsymbol{p}$ scheme was extended to the study of effects of strong and short-range impurity potentials.[27)] The scattering matrix obtained analytically shows a rule of the conductance quantization in the limit of strong scatterers that the conductance vanishes for $|\Delta N_{AB}|\geq 2$ and is quantized into one and two times $e^2/\pi\hbar$ for $|\Delta N_{AB}|=1$ and 0, respectively, where ΔN_{AB} is difference in the number of impurities at A and B sublattices. This result is in agreement with that for the lattice-vacancy obtained numerically in a tight-binding model.[16, 28-32)] See ref. 33 for a review on the effective-mass description.

In the presence of a magnetic field perpendicular to the axis, the band structure is known to be strongly modified due to a formation of two dimensional Landau states.[34-36)] This leads to various peculiar electronic properties including transport.[37-39)] Therefore, the magnetic field is expected to have a strong influence on the conductance in the presence of short-range impurities. In fact, the conductance in the presence of a simple lattice-vacancy has been shown to exhibit strong dependence on ΔN_{AB} in a magnetic field.[28, 32)] A peculiar feature is the existence of the universal dependence on the field component in the direction of the vacancy, which will be called conductance scaling in the following.

The outline of the paper is as follows: A formalism of a perturbation approach for calculating the T matrix in a magnetic field based on an effective-mass theory is developed and origin of the conductance scaling is described in the §2. In §3, we present analytical results of magnetoconductance and give general discussions in a weak and a strong-field limit. Results of numerical calculation using an effective-mass theory and a tight-binding model are given in §4. Section 5 is devoted to summary and discussion.

§2. Effective Mass Approximation

2.1 Hamiltonian

We show the lattice structure of a graphite sheet and its first Brillouin zone in Fig. 1 with the definition of coordinates. A unit cell has two carbon atoms denoted by A and B, and $\boldsymbol{L}$ and η are the chiral vector and angle, respectively.

Electronic structure of a graphite sheet near the Fermi level consists of π-π^* bands. These two bands have conical dispersion and touch at K and K' point in the first Brillouin zone. The Shrödinger equation near the Fermi level within an effective-mass scheme is given by

$$\mathcal{H}\boldsymbol{F}(\boldsymbol{r}) = \varepsilon \boldsymbol{F}(\boldsymbol{r}),$$
$$\mathcal{H} = \mathcal{H}_0 + V, \tag{2.1}$$

where $\mathcal{H}_0$ is a $\boldsymbol{k}\cdot\boldsymbol{p}$ Hamiltonian for an ideal graphite sheet, V is impurity potential, and $\boldsymbol{F}(\boldsymbol{r})$ is an envelope function. Hamiltonian is given by the following 4×4 matrix,

$$\mathcal{H}_0 = \gamma \begin{pmatrix} KA & K'A & KB & K'B \\ 0 & 0 & \hat{k}_x - \mathrm{i}\hat{k}_y & 0 \\ 0 & 0 & 0 & \hat{k}_x + \mathrm{i}\hat{k}_y \\ \hat{k}_x + \mathrm{i}\hat{k}_y & 0 & 0 & 0 \\ 0 & \hat{k}_x - \mathrm{i}\hat{k}_y & 0 & 0 \end{pmatrix}, \tag{2.2}$$

where γ is a band parameter and $\hat{\boldsymbol{k}} = (\hat{k}_x, \hat{k}_y)$ is a wave vector operator defined by

$$\hat{\boldsymbol{k}} = -\mathrm{i}\boldsymbol{\nabla} + \frac{e}{c\hbar}\boldsymbol{A}. \tag{2.3}$$

Effect of a magnetic field is included through vector potential $\boldsymbol{A}$. In this study, we deal with a magnetic field perpendicular to the axis. This leads to

$$\boldsymbol{A} = (A_x, A_y) = \left(0, \frac{LH}{2\pi}\sin\frac{2\pi}{L}x\right), \tag{2.4}$$

within the Landau gauge, where L is the circumference and H is the strength of the field.

We consider the impurity potential used in the former study,[27] which is given by

$$V = \sum_j \sum_{\alpha=A,B} V_j^{\alpha}\delta(\boldsymbol{r} - \boldsymbol{r}_j), \tag{2.5}$$

with

$$V_j^A = \begin{pmatrix} 2u_j^A \boldsymbol{a}_j \boldsymbol{a}_j^+ & 0 \\ 0 & 0 \end{pmatrix}, \quad V_j^B = \begin{pmatrix} 0 & 0 \\ 0 & 2u_j^B \boldsymbol{b}_j \boldsymbol{b}_j^+ \end{pmatrix}, \tag{2.6}$$

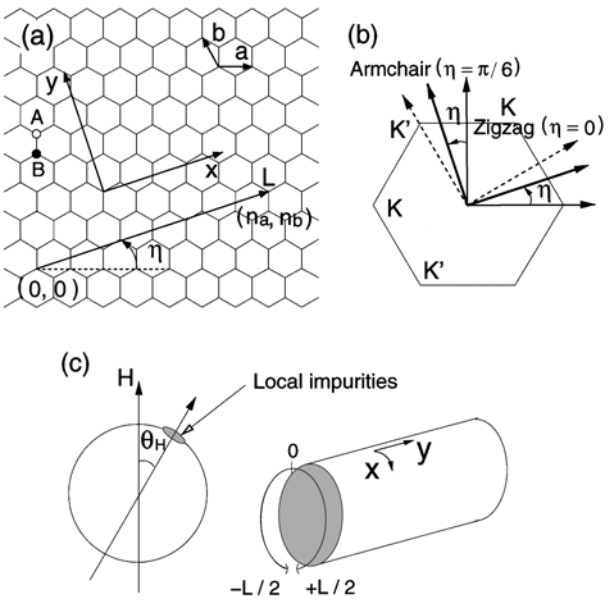

Fig. 1. (a) Lattice structure of a graphite sheet. η is the chiral angle. The coordinates are chosen in such a way that x is along the circumference of a nanotube and y is along the axis. (b) The first Brllouin zone and K and K' points. (c) The coordinates for a nanotube and definition of the angle θ_H.

where u_j^A and u_j^B are the strength of a δ function potential at an A site $\boldsymbol{r}_j$ and a B site $\boldsymbol{r}_j$, respectively, and we have defined vectors $\boldsymbol{a}_j$ and $\boldsymbol{b}_j$ as

$$\boldsymbol{a}_j = \frac{1}{\sqrt{2}}\begin{pmatrix} a_{jK} \\ a_{jK'} \end{pmatrix} = \frac{1}{\sqrt{2}}\begin{pmatrix} \mathrm{e}^{\mathrm{i}\phi_j^A/2} \\ \mathrm{e}^{-\mathrm{i}\phi_j^A/2} \end{pmatrix},$$
$$\boldsymbol{b}_j = \frac{1}{\sqrt{2}}\begin{pmatrix} b_{jK} \\ b_{jK'} \end{pmatrix} = \frac{1}{\sqrt{2}}\begin{pmatrix} \mathrm{e}^{\mathrm{i}\phi_j^B/2} \\ \mathrm{e}^{-\mathrm{i}\phi_j^B/2} \end{pmatrix}, \tag{2.7}$$

with

$$\phi_j^A = (\boldsymbol{K}' - \boldsymbol{K})\cdot\boldsymbol{r}_j + \eta,$$
$$\phi_j^B = (\boldsymbol{K}' - \boldsymbol{K})\cdot\boldsymbol{r}_j - \eta + \pi/3. \tag{2.8}$$

where $\boldsymbol{K}$ and $\boldsymbol{K}'$ are the wave vectors at K and K' points, respectively.

2.2 Landau wave function at ε=0

The $\boldsymbol{k}\cdot\boldsymbol{p}$ Hamiltonian $\mathcal{H}_0$ in the presence of a magnetic field is related to $\mathcal{H}_0^0$ in its absence through

$$\mathcal{H}_0 = P(\boldsymbol{r})^{-1}\,\mathcal{H}_0^0\,P(\boldsymbol{r})^{-1}, \tag{2.9}$$

where $P(\boldsymbol{r})$ is a diagonal matrix defined by

$$P(\boldsymbol{r}) = \begin{pmatrix} \mathrm{e}^{-f(\alpha,x)} & 0 & 0 & 0 \\ 0 & \mathrm{e}^{f(\alpha,x)} & 0 & 0 \\ 0 & 0 & \mathrm{e}^{f(\alpha,x)} & 0 \\ 0 & 0 & 0 & \mathrm{e}^{-f(\alpha,x)} \end{pmatrix}, \tag{2.10}$$

with

$$f(\alpha, x) = \alpha\cos\frac{2\pi x}{L}, \tag{2.11}$$

$$\alpha = \left(\frac{L}{2\pi l}\right)^2, \tag{2.12}$$

and l being the magnetic length defined by $l \equiv \sqrt{c\hbar/eH}$.

With the use of the above relation between $\mathcal{H}_0$ and $\mathcal{H}_0^0$, Landau wave functions at ε=0 are determined exactly.[37,38] They are given by

$$\boldsymbol{F}_{K\pm}(\boldsymbol{r}) = \frac{1}{\sqrt{AL}}\boldsymbol{f}_{K\pm}(\boldsymbol{r}), \quad \boldsymbol{F}_{K'\pm}(\boldsymbol{r}) = \frac{1}{\sqrt{AL}}\boldsymbol{f}_{K'\pm}(\boldsymbol{r}), \tag{2.13}$$

where A is the length of CN and

$$\boldsymbol{f}_{K\pm}(\boldsymbol{r}) = \begin{bmatrix} F^-(\boldsymbol{r}) \\ 0 \\ \pm \mathrm{i}F^+(\boldsymbol{r}) \\ 0 \end{bmatrix}, \quad \boldsymbol{f}_{K'\pm}(\boldsymbol{r}) = \begin{bmatrix} 0 \\ F^+(\boldsymbol{r}) \\ 0 \\ \mp \mathrm{i}F^-(\boldsymbol{r}) \end{bmatrix}, \tag{2.14}$$

with

$$F^{\pm}(\boldsymbol{r}) = \frac{1}{\sqrt{2I_0(\alpha)}} \exp\left[\pm f(\alpha, x)\right], \tag{2.15}$$

and $I_0(z)$ being the modified Bessel function defined as

$$I_0(z) = \frac{1}{\pi}\int \mathrm{d}\theta \exp(z\cos\theta). \tag{2.16}$$

The effective strength of the field is characterized by the parameter α. We have two regimes, a weak-field regime $\alpha \ll 1$ and a strong-field regime $\alpha \gg 1$. In the strong-field regime, $F^+(\boldsymbol{r})$ and $F^-(\boldsymbol{r})$ are localized around x=0 and x=$\pm L/2$, i.e., top and bottom of CN's, respectively. Because of this localized feature of the Landau wave function, envelope functions for A and B sites do not overlap each other in the strong-field regime. The group velocity at ε=0 is given by

$$v = \frac{\hbar}{\gamma I_0(\alpha)}. \tag{2.17}$$

In the following we shall mainly confine ourselves to the case ε=0 where analytic expressions can be obtained for the wave functions and Green's functions. The extension to the case $\varepsilon \neq 0$ is straightforward except that numerical calculations are required for wave functions and Green's functions.

2.3 Green's function at ε=0

One particle Green's function at $\varepsilon = 0$ is defined by

$$[\mathrm{i}0 - \mathcal{H}_0]G = [\mathrm{i}0 - P^{-1}\mathcal{H}_0^0 P^{-1}]G = 1. \tag{2.18}$$

In terms of Green's function G^0 in the absence of a magnetic field, given by $[\mathrm{i}0 - \mathcal{H}_0^0]\, G^0$=1, we have

$$G = PG^0P. \tag{2.19}$$

In r-representation, this becomes

$$G_{jj'} = P(\boldsymbol{r}_j)G^0_{jj'}P(\boldsymbol{r}_{j'}). \tag{2.20}$$

With the use of Green's function obtained previously in the absence of a magnetic field,[27] we have explicitly

$$G_{jj'} = \frac{-\mathrm{i}A}{2\gamma}\begin{pmatrix} \boldsymbol{G}^{AA}_{jj'} & \boldsymbol{G}^{AB}_{jj'} \\ \boldsymbol{G}^{BA}_{jj'} & \boldsymbol{G}^{BB}_{jj'} \end{pmatrix}, \tag{2.21}$$

with

$$\boldsymbol{G}^{AA}_{jj'} = \begin{pmatrix} g_0^- & 0 \\ 0 & g_0^+ \end{pmatrix}, \quad \boldsymbol{G}^{BB}_{jj'} = \begin{pmatrix} g_0^+ & 0 \\ 0 & g_0^- \end{pmatrix},$$
$$\boldsymbol{G}^{AB}_{jj'} = \begin{pmatrix} g_1 & 0 \\ 0 & \bar{g}_1 \end{pmatrix}, \quad \boldsymbol{G}^{BA}_{jj'} = \begin{pmatrix} \bar{g}_1 & 0 \\ 0 & g_1 \end{pmatrix}, \tag{2.22}$$

where

$$g_0^{\pm}(\boldsymbol{r}_j, \boldsymbol{r}_{j'}) = \exp\left[\pm(f_j + f_{j'})\right] g_0(\boldsymbol{r}_{jj'}),$$
$$g_1(\boldsymbol{r}_j, \boldsymbol{r}_{j'}) = \exp\left[-(f_j - f_{j'})\right] g_1(\boldsymbol{r}_{jj'}),$$
$$\bar{g}_1(\boldsymbol{r}_j, \boldsymbol{r}_{j'}) = \exp\left[+(f_j - f_{j'})\right] g_1^*(\boldsymbol{r}_{jj'}), \tag{2.23}$$

and $\boldsymbol{r}_{jj'}$=$\boldsymbol{r}_j$−$\boldsymbol{r}_{j'}$. The diagonal Green's function $g_0^{\pm}$ represents propagation among same sublattice points and the off-diagonal terms g_1 and $\bar{g}_1$ represent propagation between different sublattices. In the above equation, we have introduced

$$f_j \equiv f(\alpha, x_j), \tag{2.24}$$

and the diagonal and off-diagonal Green's functions in the absence of a magnetic field,

$$g_0(\boldsymbol{r}_{jj'}) = 1, \tag{2.25}$$

$$g_1(\boldsymbol{r}_{jj'}) = \frac{\cos[\pi(x + \mathrm{i}y)/L]}{\sin[\pi(x + \mathrm{i}y)/L]}. \tag{2.26}$$

with x=x_j−$x_{j'}$ and y=y_j−$y_{j'}$. When impurities are localized within a distance of a few times of the lattice constant, $g_1(\boldsymbol{r}_{jj'})$ becomes extremely large. This singular behavior is the origin of the conductance quantization of CN's with the local lattice-vacancy which we have already discussed in the former study.[27]

In the perturbation expansion of the T matrix, diagonal and off-diagonal Green's functions always appear only between matrix elements of impurities and therefore in the form

$$\begin{aligned} \boldsymbol{a}_j^+ \boldsymbol{G}^{AA}_{jj'}\boldsymbol{a}_{j'} &= (\boldsymbol{a}_j, \boldsymbol{a}_{j'})\, \tilde{g}^{AA}_{jj'}, \\ \boldsymbol{b}_j^+ \boldsymbol{G}^{BB}_{jj'}\boldsymbol{b}_{j'} &= (\boldsymbol{b}_j, \boldsymbol{b}_{j'})\, \tilde{g}^{BB}_{jj'}, \\ \boldsymbol{a}_j^+ \boldsymbol{G}^{AB}_{jj'}\boldsymbol{b}_{j'} &= (\boldsymbol{a}_j, \boldsymbol{b}_{j'})\, \tilde{g}^{AB}_{jj'}, \\ \boldsymbol{b}_j^+ \boldsymbol{G}^{BA}_{jj'}\boldsymbol{a}_{j'} &= (\boldsymbol{b}_j, \boldsymbol{a}_{j'})\, \tilde{g}^{BA}_{jj'}, \end{aligned} \tag{2.27}$$

with

$$\begin{aligned} \tilde{g}^{AA}_{jj'} &= \cosh[f_j + f_{j'}] + \mathrm{i}\sinh[f_j + f_{j'}]\tan[\phi^{AA}_{jj'}], \\ \tilde{g}^{BB}_{jj'} &= \cosh[f_j + f_{j'}] - \mathrm{i}\sinh[f_j + f_{j'}]\tan[\phi^{BB}_{jj'}], \\ \tilde{g}^{AB}_{jj'} &= \frac{1}{2}\left[g_1(\boldsymbol{r}_{jj'})\mathrm{e}^{-[f_j - f_{j'}]}\mathrm{e}^{-\mathrm{i}\phi^{AB}_{jj'}}\right. \\ &\quad \left. + g_1^*(\boldsymbol{r}_{jj'})\mathrm{e}^{[f_j - f_{j'}]}\mathrm{e}^{\mathrm{i}\phi^{AB}_{jj'}}\right](\boldsymbol{a}_i, \boldsymbol{b}_j)^{-1}, \\ \tilde{g}^{BA}_{jj'} &= \frac{1}{2}\left[g_1^*(\boldsymbol{r}_{jj'})\mathrm{e}^{[f_j - f_{j'}]}\mathrm{e}^{-\mathrm{i}\phi^{BA}_{jj'}}\right. \\ &\quad \left. + g_1(\boldsymbol{r}_{jj'})\mathrm{e}^{-[f_j - f_{j'}]}\mathrm{e}^{\mathrm{i}\phi^{BA}_{jj'}}\right](\boldsymbol{b}_i, \boldsymbol{a}_j)^{-1}, \end{aligned} \tag{2.28}$$

where $\phi^{\alpha\beta}_{jj'}$=$(\phi^{\alpha}_j - \phi^{\alpha}_{j'})/2$ (α, β = A or B). This means that we can always use $\tilde{g}^{\alpha\beta}_{jj'}$ for Green's function describing the propagation from a β site at $\boldsymbol{r}_{j'}$ to an α site at $\boldsymbol{r}_j$.

2.4 Scattering matrix

The scattering matrix can be written formally as

$$S = S^{(0)} + S^{(1)}, \tag{2.29}$$

with

$$[S^{(0)}]_{\alpha\beta} = \delta_{\alpha\beta}, \tag{2.30}$$

$$[S^{(1)}]_{\alpha\beta} = -\mathrm{i}\frac{A}{\hbar\sqrt{v_\alpha v_\beta}}T_{\alpha\beta}, \tag{2.31}$$

where v_α and v_β are velocity of channels α and β, respectively, and T is a T matrix defined by

$$T = V + VGV + VGVGV + \cdots = V + VGT. \tag{2.32}$$

In the k-representation, eq. (2.32) becomes

$$T_{\alpha\beta} = \sum_{ij} \boldsymbol{f}_\alpha^+(\boldsymbol{r}_i) T_{ij} \boldsymbol{f}_\beta(\boldsymbol{r}_j), \tag{2.33}$$

with

$$T_{ij} = \Big[\Big(1 - \frac{1}{AL}VG\Big)^{-1}\frac{1}{AL}V\Big]_{ij}, \tag{2.34}$$

where the summation is taken over all impurities and T_{ij} is the T matrix in the r-representation.

The equation for T_{ij} is given by

$$T_{ij} = \frac{1}{AL}V_i\delta_{ij} + \frac{1}{AL}V_i\sum_k G_{ik}T_{kj} \tag{2.35}$$

Effect of the multiple scattering from a single impurity is exactly taken into account by introducing renormalized potential $\tilde{V}$ by

$$\tilde{V}_i = \Big[1 - \frac{1}{AL}V_iG_{ii}\Big]^{-1}V_i \tag{2.36}$$

Then the equation for T_{ij} can be rewritten with use of $\tilde{V}$ as

$$T_{ij} = \frac{1}{AL}\tilde{V}_i\delta_{ij} + \frac{1}{AL}\tilde{V}_i\sum_{k\neq i} G_{ik}T_{kj}. \tag{2.37}$$

In general, we can write

$$T_{ij} = \begin{pmatrix} T_{ij}^{AA} & T_{ij}^{AB} \\ T_{ij}^{BA} & T_{ij}^{BB} \end{pmatrix}, \tag{2.38}$$

in terms of $(2,2)$ matrices T_{ij}^{AA}, etc.

When $\varepsilon = 0$, metallic CN's always have two open channels at K and K' point. Therefore we can write the scattering matrix as

$$S = \begin{pmatrix} r_{KK} & r_{KK'} & t'_{KK} & t'_{KK'} \\ r_{K'K} & r_{K'K'} & t'_{K'K} & t'_{K'K'} \\ t_{KK} & t_{KK'} & r'_{KK} & r'_{KK'} \\ t_{K'K} & t_{K'K'} & r'_{K'K} & r'_{K'K'} \end{pmatrix}, \tag{2.39}$$

where t's and r's are transmission and reflection coefficients, respectively.

Using the Landau wave function at $\varepsilon = 0$, $S^{(1)}$ can be written as

$$S_{\alpha\beta}^{(1)} = -\mathrm{i}\frac{A}{\gamma}I_0(\alpha)\sum_{ij}\boldsymbol{f}_\alpha(\boldsymbol{r}_i)^+ T_{ij}\,\boldsymbol{f}_\beta(\boldsymbol{r}_j), \tag{2.40}$$

where summation is taken over all combination of impurities. Once transmission coefficients are obtained, conductance is calculated by Landauer formula,[40] given by

$$G = \frac{e^2}{\pi\hbar}\sum_{\mu,\nu}|t_{\mu\nu}|^2, \tag{2.41}$$

where combinations of $\{\mu,\nu\}$ are given by $\{K,K\}$, $\{K',K'\}$, $\{K',K\}$, and $\{K,K'\}$. The former two correspond to intra-valley scattering and the latter two correspond to inter-valley scattering between K and K' points.

2.5 Scaling of conductance

In the following we shall confine ourselves to the case that impurities are localized within a range smaller than circumference of CN, i.e., $|\boldsymbol{r}_j - \boldsymbol{r}_{j'}| \ll L$, at $\varepsilon = 0$. Then, equation (2.23) can be rewritten as

$$\begin{aligned} g_0^{\pm}(\boldsymbol{r}_j, \boldsymbol{r}_{j'}) &= \exp[\pm 2f_0], \\ g_1\,(\boldsymbol{r}_j, \boldsymbol{r}_{j'}) &= g_1(\boldsymbol{r}_{jj'}), \\ \bar{g}_1\,(\boldsymbol{r}_j, \boldsymbol{r}_{j'}) &= g_1^*(\boldsymbol{r}_{jj'}), \end{aligned} \tag{2.42}$$

with $f_0 = f(\alpha, x_0)$, where $\boldsymbol{r}_0{=}(x_0, y_0)$ is the center-of-mass of impurities. In eq. (2.42), effects of the magnetic field appear only in the diagonal Green's function which is determined by the local density of states at $\boldsymbol{r}_0$.

We can also replace eq. (2.40) by

$$S_{\alpha\beta}^{(1)} = -\mathrm{i}\frac{A}{\gamma}\,I_0(\alpha)\,\boldsymbol{f}_\alpha(\boldsymbol{r}_0)^+\,T_{\mathrm{S}}\,\boldsymbol{f}_\beta(\boldsymbol{r}_0), \tag{2.43}$$

with

$$T_{\mathrm{S}} = \sum_{ij} T_{ij}. \tag{2.44}$$

The factor $I_0(\alpha)$ appearing in eq. (2.43) is canceled by the normalization factor of the wave function $\boldsymbol{F}$ as in eq. (2.15). Therefore, the magnetic field appears in the S matrix only in the form $f_0 = f(\alpha, x_0)$. Because $f(\alpha, x_0) = (L/2\pi l)^2\cos\theta_H$ with $\theta_H = 2\pi x_0/L$, this means that the S matrix depends only on the field component $H\cos\theta_H$ in the direction perpendicular to the nanotube surface at the center-of-mass of impurities. This is the origin of the scaling law of conductance which we found in a previous numerical study.[28, 32]

In this case, the Green's functions are rewritten as

$$\begin{aligned} \tilde{g}_{jj'}^{AA} &= \cosh[2f_0] + \mathrm{i}\sinh[2f_0]\tan(\phi_{jj'}^{AA}), \\ \tilde{g}_{jj'}^{BB} &= \cosh[2f_0] - \mathrm{i}\sinh[2f_0]\tan(\phi_{jj'}^{BB}), \\ \tilde{g}_{jj'}^{AB} &= \mathrm{Re}\big[g_1(\boldsymbol{r}_{jj'})\mathrm{e}^{-\mathrm{i}\tilde{\phi}_{jj'}^{AB}}\big](\boldsymbol{a}_j, \boldsymbol{b}_{j'})^{-1}, \\ \tilde{g}_{jj'}^{BA} &= \mathrm{Re}\big[g_1^*(\boldsymbol{r}_{jj'})\mathrm{e}^{-\mathrm{i}\tilde{\phi}_{jj'}^{BA}}\big](\boldsymbol{b}_j, \boldsymbol{a}_{j'})^{-1}. \end{aligned} \tag{2.45}$$

2.6 T matrix

In the following, we shall exclusively consider the case that all impurities have a same strength, i.e., $u_j{=}u$. An extension to other cases is straightforward. By using eq. (2.36), the renormalized impurity potential can be written as

$$u \to \frac{\gamma L}{\mathrm{i}\tilde{g}_0}\zeta, \tag{2.46}$$

with

$$\tilde{g}_0 = \tilde{g}_{jj}^{AA} = \tilde{g}_{jj}^{BB} = \cosh[2f(\alpha, x_0)], \tag{2.47}$$

$$\zeta = \frac{1}{1 + (2\mathrm{i}\tilde{u}\tilde{g}_0)^{-1}}, \tag{2.48}$$

$$\tilde{u} = \frac{u}{2\gamma L}. \tag{2.49}$$

An examination of perturbation series with respect to the impurity potential reveals that the T matrix can be written as

$$\begin{aligned} T_{ij}^{AA} &= \frac{1}{AL}\frac{\gamma L}{\mathrm{i}\tilde{g}_0}\zeta 2\boldsymbol{a}_i\boldsymbol{a}_j^+ t_{ij}^{AA}, \\ T_{ij}^{BB} &= \frac{1}{AL}\frac{\gamma L}{\mathrm{i}\tilde{g}_0}\zeta 2\boldsymbol{b}_i\boldsymbol{b}_j^+ t_{ij}^{BB}, \\ T_{ij}^{AB} &= \frac{1}{AL}\frac{\gamma L}{\mathrm{i}\tilde{g}_0}\zeta 2\boldsymbol{a}_i\boldsymbol{b}_j^+ t_{ij}^{AB}, \\ T_{ij}^{BA} &= \frac{1}{AL}\frac{\gamma L}{\mathrm{i}\tilde{g}_0}\zeta 2\boldsymbol{b}_i\boldsymbol{a}_j^+ t_{ij}^{BA}. \end{aligned} \tag{2.50}$$

As a result the equations for the T matrix can formally be written as

$$\begin{aligned} (1-\zeta+\zeta\tilde{g}_0^{-1}\varGamma^{AA})t^{AA} &= 1-\zeta\tilde{g}_0^{-1}\varGamma^{AB}t^{BA}, \\ (1-\zeta+\zeta\tilde{g}_0^{-1}\varGamma^{BB})t^{BB} &= 1-\zeta\tilde{g}_0^{-1}\varGamma^{BA}t^{AB}, \\ (1-\zeta+\zeta\tilde{g}_0^{-1}\varGamma^{AA})t^{AB} &= -\zeta\tilde{g}_0^{-1}\varGamma^{AB}t^{BB}, \\ (1-\zeta+\zeta\tilde{g}_0^{-1}\varGamma^{BB})t^{BA} &= -\zeta\tilde{g}_0^{-1}\varGamma^{BA}t^{AA}, \end{aligned} \tag{2.51}$$

where we define the following matrices:

$$\begin{aligned} t^{AA} &= (t_{ij}^{AA}), \quad t^{BB} = (t_{ij}^{BA}), \\ t^{AB} &= (t_{ij}^{AA}), \quad t^{BA} = (t_{ij}^{BA}), \\ \varGamma^{AA} &= (\varGamma_{ij}^{AA}), \quad \varGamma^{BB} = (\varGamma_{ij}^{BB}), \\ \varGamma^{AB} &= (\varGamma_{ij}^{AB}), \quad \varGamma^{BA} = (\varGamma_{ij}^{BA}), \end{aligned} \tag{2.52}$$

with

$$\begin{aligned} \varGamma_{ij}^{AA} &= \tilde{g}_{ij}^{AA}\boldsymbol{a}_i^+\boldsymbol{a}_j, \quad \varGamma_{ij}^{BB} = \tilde{g}_{ij}^{BB}\boldsymbol{b}_i^+\boldsymbol{b}_j, \\ \varGamma_{ij}^{AB} &= \tilde{g}_{ij}^{AB}\boldsymbol{a}_i^+\boldsymbol{b}_j, \quad \varGamma_{ij}^{BA} = \tilde{g}_{ij}^{BA}\boldsymbol{b}_i^+\boldsymbol{a}_j. \end{aligned} \tag{2.53}$$

If there are N_A and N_B impurities at A and B site, respectively, t^{AA} and $\varGamma^{AA}$ are an (N_A, N_A) matrix, t^{BB} and $\varGamma^{BB}$ are an (N_B, N_B) matrix, t^{AB} and $\varGamma^{AB}$ are an (N_A, N_B) matrix, and t^{BA} and $\varGamma^{BA}$ are an (N_B, N_A) matrix. In the case of a finite number of impurities, we solve eq. (2.51) numerically and obtain T matrix using eq. (2.50). The above equations are essentially same as those in the absence of a magnetic field, and the magnetic field appears mainly through the change in the diagonal Green's function from g_0 to $\tilde{g}_0 = \cosh[2f(\alpha, x_0)]$.

We write the summation of T_{ij} as

$$T_{\mathrm{S}} = \begin{pmatrix} T^{AA} & T^{AB} \\ T^{BA} & T^{BB} \end{pmatrix}, \tag{2.54}$$

where T^{AA}, T^{AB}, T^{BA}, and T^{BB} are $(2,2)$ matrices given by

$$T^{AA} = \begin{pmatrix} T_{KK}^{AA} & T_{KK'}^{AA} \\ T_{K'K}^{AA} & T_{K'K'}^{AA} \end{pmatrix}, \quad \text{etc.} \tag{2.55}$$

Then, the reflection coefficients are given by

$$\begin{aligned} r_{KK} &= \frac{-\mathrm{i}A}{2\gamma}\left(\mathrm{e}^{-2f_0}T_{KK}^{AA} - \mathrm{e}^{2f_0}T_{KK}^{BB} + \mathrm{i}T_{KK}^{AB} + \mathrm{i}T_{KK}^{BA}\right), \\ r_{K'K'} &= \frac{-\mathrm{i}A}{2\gamma}\left(\mathrm{e}^{2f_0}T_{K'K'}^{AA} - \mathrm{e}^{-2f_0}T_{K'K'}^{BB}\right. \\ &\qquad \left. -\mathrm{i}T_{K'K'}^{AB} - \mathrm{i}T_{K'K'}^{BA}\right), \\ r_{K'K} &= \frac{-\mathrm{i}A}{2\gamma}\left(T_{K'K}^{AA} + T_{K'K}^{BB} + \mathrm{i}\mathrm{e}^{2f_0}T_{K'K}^{AB} - \mathrm{i}\mathrm{e}^{-2f_0}T_{K'K}^{BA}\right), \\ r_{KK'} &= \frac{-\mathrm{i}A}{2\gamma}\left(T_{AA}^{KK'} + T_{BB}^{KK'} - \mathrm{i}\mathrm{e}^{-2f_0}T_{KK'}^{AB} + \mathrm{i}\mathrm{e}^{2f_0}T_{KK'}^{BA}\right), \end{aligned} \tag{2.56}$$

and the transmission coefficients are given by

$$\begin{aligned} t_{KK} &= 1 + \frac{-\mathrm{i}A}{2\gamma}\left(\mathrm{e}^{-2f_0}T_{KK}^{AA} + \mathrm{e}^{2f_0}T_{KK}^{BB} + \mathrm{i}T_{KK}^{AB} - \mathrm{i}T_{KK}^{BA}\right), \\ t_{K'K'} &= 1 + \frac{-\mathrm{i}A}{2\gamma}\left(\mathrm{e}^{2f_0}T_{K'K'}^{AA} + \mathrm{e}^{-2f_0}T_{K'K'}^{BB}\right. \\ &\qquad \left. -\mathrm{i}T_{K'K'}^{AB} + \mathrm{i}T_{K'K'}^{BA}\right), \\ t_{K'K} &= \frac{-\mathrm{i}A}{2\gamma}\left(T_{K'K}^{AA} - T_{K'K}^{BB} + \mathrm{i}\mathrm{e}^{2f_0}T_{K'K}^{AB} + \mathrm{i}\mathrm{e}^{-2f_0}T_{K'K}^{BA}\right), \\ t_{KK'} &= \frac{-\mathrm{i}A}{2\gamma}\left(T_{KK'}^{AA} - T_{KK'}^{BB} - \mathrm{i}\mathrm{e}^{-2f_0}T_{KK'}^{AB} - \mathrm{i}\mathrm{e}^{2f_0}T_{KK'}^{BA}\right). \end{aligned} \tag{2.57}$$

Similar expressions are obtained for r'_{KK}, etc. and t'_{KK}, etc. for waves incident from the right hand side.

§3. Examples

In the following, the center-of-mass of impurities is always chosen at $\boldsymbol{r}_0$=0 and θ_H=0, i.e, a top of CN's, for simplicity. The conductance for arbitrarily values of θ_H is obtained by replacing the strength of magnetic field H by $H\cos\theta_H$ because of the scaling shown above.

3.1 Impurities at same sublattices

We first consider the case where N_A impurities are introduced at A sites within the distance much smaller than L. In this case, only the diagonal Green's function $g_0^{\pm}(\boldsymbol{r}, \boldsymbol{r}')$ appears in the perturbation series for the T matrix. Because $g_0^{\pm}(\boldsymbol{r}, \boldsymbol{r}')$ does not vary with the distance so much, it can be replaced by $g_0^{\pm}(\boldsymbol{r}_0, \boldsymbol{r}_0)$, where $\boldsymbol{r}_0$ is the center-of-mass of impurities. As a result T matrices are given by T^{AB}=T^{BA}=T^{BB}=0 and

$$T^{AA} = V_{\mathrm{S}}^A + V_{\mathrm{S}}^A G_{00}^{AA} T^{AA}, \tag{3.1}$$

with

$$V_{\mathrm{S}}^A = \sum_j 2\tilde{u}_j \boldsymbol{a}_j \boldsymbol{a}_j^+, \tag{3.2}$$

where G_{00}^{AA} is diagonal Green's function at the center-of-mass of impurities. This result shows that the effective potential for localized impurities is given by the sum of their potentials.

We write a position of impurity at an A site as $\boldsymbol{r}_j^A = n_{aj}\boldsymbol{a} + n_{bj}\boldsymbol{b}$, where $\boldsymbol{a}$ and $\boldsymbol{b}$ are primitive lattice translation vectors shown in Fig. 1 and n_{aj} and n_{bj} are integers. For this lattice point, ϕ_j^A is given by

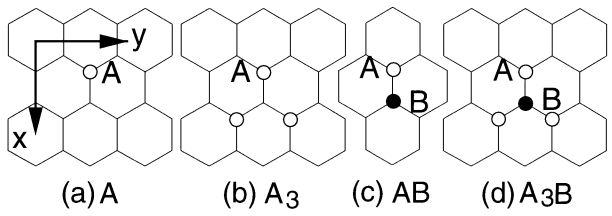

Fig. 2. Schematic illustration of impurities in an armchair nanotube. The open and closed circles denote A and B lattice points, respectively. (a) A, (b) A_3, (c) AB, and (d) A_3B.

$$\phi_j^A = (\boldsymbol{K}' - \boldsymbol{K}) \cdot (n_{aj}\boldsymbol{a} + n_{bj}\boldsymbol{b}) + \eta = \frac{2\pi}{3}(n_{aj} + n_{bj}) + \eta \pmod{2\pi}. \tag{3.3}$$

It is obvious from eq. (3.3) that ϕ_j^A takes only three independent values η, $\eta + 2\pi/3$ or $\eta + 4\pi/3$.

If there are N_1 impurities with $\phi_1^A{=}\eta$, N_2 impurities with $\phi_2^A{=}\eta{+}2\pi/3$, and N_3 impurities with $\phi_3^A{=}\eta{+}4\pi/3$, T^{AA} is given by

$$T^{AA} = \frac{2\gamma}{\mathrm{i}A}\frac{\mathrm{i}\tilde{u}}{1 - 3M\tilde{u}^2 + 2\mathrm{i}N\tilde{u}\tilde{g}_0} \times \begin{pmatrix} N{+}3\mathrm{i}M\tilde{u}\mathrm{e}^{2f_0} & \mathrm{e}^{\mathrm{i}\eta}P \\ \mathrm{e}^{-\mathrm{i}\eta}P^* & N{+}3\mathrm{i}M\tilde{u}\mathrm{e}^{-2f_0} \end{pmatrix}, \tag{3.4}$$

with

$$N = N_1 + N_2 + N_3, \quad M = N_1N_2 + N_2N_3 + N_3N_1, \quad P = N_1 + N_2\,\omega + N_3\,\omega^{-1}, \tag{3.5}$$

where $\omega{=}\exp(2\pi i/3)$. When $N_1{=}N_2{=}N_3$, P vanishes and inter-valley transmission and reflection become absent. From eq. (3.4) we obtain an analytical expression for the conductance

$$G = \frac{e^2}{\pi\hbar}\Big(1 + \frac{1 - (3\tilde{u}^2M)^2}{(1 - 3\tilde{u}^2M)^2 + (2N\tilde{u}\tilde{g}_0)^2}\Big). \tag{3.6}$$

The conductance is independent of the parameter P.

This shows that the conductance is always quantized into the conductance quantum $e^2/\pi\hbar$ (a half of the ideal conductance) and independent of N and M in the strong-field limit $\tilde{g} \to \infty$. Its origin is intuitively understood by the distribution of Landau wave functions along the circumference direction. In fact, the Landau wave function at the K' point is mainly localized in the A site at a top of CN's. When impurities exist in the A site at the top of CN's, a scattering probability for an in-coming channel K' increases due to the multiple scattering among the A sites and consequently the in-coming wave is reflected back into the same valley, i.e., $r_{K'K'} = 1$. At the K point, the situation is completely opposite and the Landau wave function for the A site has no amplitude at the top of CN's. This leads to a complete transmission for the wave at the K point. Therefore the conductance is quantized into the conductance quantum in the strong-field limit. For impurities at B sites, the same conductance is obtained except that the roles of the K and K' points are interchanged.

For a single impurity with $N_1 = 1$ and $N_2 = N_3 = 0$, in particular, we have

$$G = \frac{e^2}{\pi\hbar}\Big(1 + \frac{1}{1 + (2\tilde{u}\tilde{g}_0)^2}\Big). \tag{3.7}$$

This shows that the conductance is given by $G \approx e^2/\pi\hbar$ independent of the field in the case of a strong scatterer $|\tilde{u}|{\gg}1$. In the case of A_3 impurities $N_1 = N_2 = N_3 = 1$ [see Fig. 2 (b)], we have $N{=}3$, $M{=}3$, and $P{=}0$. In the absence of a magnetic field, a perfect reflection occurs and the conductance becomes zero in the limit of strong scatterers. In high magnetic fields, the conductance is again quantized into $e^2/\pi\hbar$.

3.2 Pair of impurities: AB

We next consider two neighboring impurities at an A site $\boldsymbol{r}_A$ and at a B site $\boldsymbol{r}_B$. In this case, the T matrix satisfies

$$\begin{aligned} t^{AA} &= 1 - \zeta\tilde{g}_0^{-1}\Gamma^{AB}t^{BA}, \\ t^{BB} &= 1 - \zeta\tilde{g}_0^{-1}\Gamma^{BA}t^{AB}, \\ t^{AB} &= -\zeta\tilde{g}_0^{-1}\Gamma^{AB}t^{BB}, \\ t^{BA} &= -\zeta\tilde{g}_0^{-1}\Gamma^{BA}t^{AA}. \end{aligned} \tag{3.8}$$

This leads to

$$t^{AA} = t^{BB} = \frac{1}{1 + (\Gamma^{AB}\zeta\tilde{g}_0^{-1})^2}, \quad t^{AB} = -t^{BA} = -\frac{\Gamma^{AB}\zeta\tilde{g}_0^{-1}}{1 + (\Gamma^{AB}\zeta\tilde{g}_0^{-1})^2}, \tag{3.9}$$

where use has been made of $\Gamma^{BA} = -\Gamma^{AB}$.

In a weak-field regime $f_0 = \alpha \ll 1$, we have $\tilde{g}_0 \sim 1$ and $|g^{AB}| \sim (L/a)$. In the case of strong scatterers, therefore, the conductance is approximately given by an ideal value $2e^2/\pi\hbar$ with small corrections,

$$G = \frac{2e^2}{\pi\hbar}\Big[1 - \frac{1}{(\Gamma^{AB})^2}\left(1 + \sin^2\phi^{AB} + 4f_0^2\right)\Big], \tag{3.10}$$

where $\phi^{AB} = (\phi^A - \phi^B)/2$. The deviation from the ideal conductance increases with the the field but its magnitude is quite small because $(\Gamma^{AB})^2 \sim (L/a)^2 \gg 1$.

In the strong-field regime $f_0 \gg 1$, the diagonal Green's function becomes extremely large, i.e., $\tilde{g}_0 = \cosh[2f_0] \simeq \exp[2f_0] \gg 1$. When the condition $\Gamma^{AB}\zeta\tilde{g}_0^{-1}{\approx}\Gamma^{AB}\tilde{g}_0^{-1}{\ll}1$ is satisfied, we have $t^{AA}{=}t^{BB}{\simeq}1$ and $t^{AB}{=}{-}t^{BA}{\simeq}{-}\Gamma^{AB}\tilde{g}_0^{-1}$. This means that we can ignore effects of off-diagonal Green's function in the strong-field limit. The conductance is given by

$$G \simeq 8\mathrm{e}^{-4f_0}(\Gamma^{AB})^2, \tag{3.11}$$

which is exponentially small.

3.3 Impurities: $A_{N_A}B_{N_B}$

Consider the general case N_A impurities at the A site and N_B impurities at the B site, where $N_A{>}0$ and $N_B{>}0$. In the absence of a magnetic field, the conductance is quantized into zero, one, and two times of the conductance quantum $e^2/\pi\hbar$ depending on the difference in the number of impurities at A and B sublattices (ΔN_{AB}) in

the case of strong scatterers and $L/a \gg 1$. This can be understood in terms of a pair-wise elimination by multiple scattering between A and B impurities as has been shown previously.[27] The situation does not change as long as the diagonal Green's function $\tilde{g}_0$ is not so much different from unity. Corrections due to the magnetic field can be calculated and in the case $\Delta N_{AB} = 0$, for example, the correction is given by

$$\Delta G \simeq -\frac{e^2}{\pi\hbar} C \Big(\frac{a}{L}\Big)^2 f_0^2, \tag{3.12}$$

where and C is a positive constant roughly proportional to $O(N_A + N_B)$.

In the strong-field where the diagonal Green's function becomes much larger than the off-diagonal term, we have

$$\begin{aligned} t^{AA} &\approx (1 - \zeta + \zeta\tilde{g}^{-1}\Gamma^{AA})^{-1}, \quad t^{AB} \approx 0, \\ t^{BB} &\approx (1 - \zeta + \zeta\tilde{g}^{-1}\Gamma^{BB})^{-1}, \quad t^{BA} \approx 0. \end{aligned} \tag{3.13}$$

Since t^{AA} and t^{BB} are same as those for impurities at same sites, reflection and transmission coefficients are solved analytically and become

$$\begin{aligned} &r_{KK} = r_{K'K'} \approx 1, \\ &r_{K'K} = r_{KK'} \approx 0, \\ &t_{KK} = t_{K'K'} = t_{K'K} = t_{KK'} \approx 0. \end{aligned} \tag{3.14}$$

These results indicate that the conductance vanishes always in the strong-field limit independent of ΔN_{AB}. This can intuitively be understood again by the buildup of the wave function at the top side of the cylindrical nanotube in high magnetic fields. In fact, the incident wave at the K' is scattered strongly by the potential at A sites and that at the K points by the potential at B sites.

There exists a magnetic field range where $\tilde{g}_0 \gg 1$ with $\tilde{g}_0 \ll |\tilde{g}^{AB}|$ and $\tilde{g}_0 \ll |\tilde{g}^{BA}|$, because $|\tilde{g}^{AB}| \sim |\tilde{g}^{BA}| \sim (L/a) \gg 1$. In such intermediate field range, scattering is determined by ΔN_{AB} remaining impurities at A or B sublattices. Therefore the conductance is given by an expression similar to eq. (3.6) for impurities only at A or B sublattice points. This shows that the conductance is nearly quantized into $e^2/\pi\hbar$ for sufficiently strong impurities with $|\tilde{u}\tilde{g}_0| \gg 1$. For $\Delta N_{AB} = 2$ such as AB_3 impurities to be discussed in the next section, for example, the conductance nearly vanishes in the absence of a magnetic field, increases and takes the value $e^2/\pi\hbar$ in the intermediate field range, and then decreases and vanishes in the limit of a strong magnetic field. For $\Delta N_{AB} = 1$ such as $A_{43}B_{42}$, on the other hand, the conductance stays at $\sim e^2/\pi\hbar$ for a wide range of the magnetic field and vanishes in the high-field limit.

§4. Numerical Calculations

The local site energy V at an impurity in a tight-binding model and the potential strength $\tilde{u}$ in the effective-mass theory are connected to each other by following relations.

$$u = \frac{\sqrt{3}}{2}a^2 V, \quad \gamma = \frac{\sqrt{3}}{2}\gamma_0 a, \quad \tilde{u} = \frac{1}{2}\frac{a}{L}\frac{V}{\gamma_0}, \tag{4.1}$$

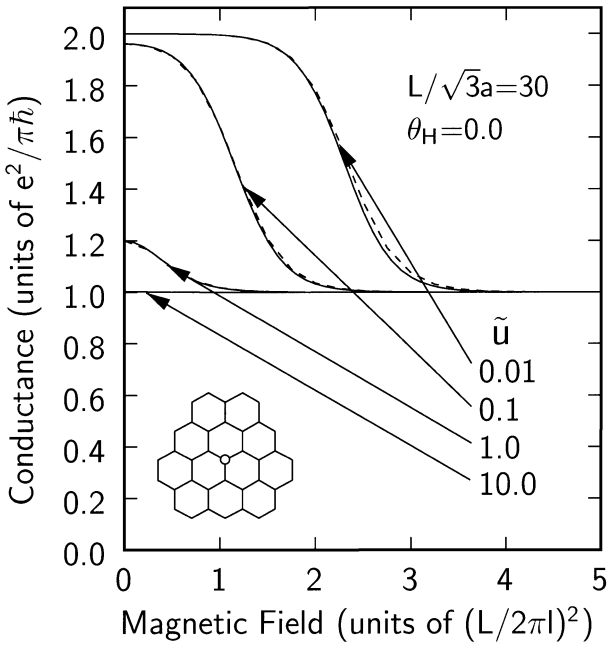

Fig. 3. Calculated conductance as a function of a magnetic field at ε=0 in the presence of a single impurity potential at an A site in armchair nanotubes for several $\tilde{u}$. $L/\sqrt{3}a$=30 and θ_H=0. Solid and dashed lines are results obtained by the effective-mass theory and in a tight-binding model, respectively.

where γ_0 is a nearest-neighbor hopping integral and a is the lattice constant. For examples, we have $V/\gamma_0 = 100$, 10, 1, and 0.1 for $\tilde{u} = 1$, 0.1, 0.01, and 0.001, respectively, when $L/a = 50$. In this section, we shall consider the case θ_H=0 and $\varepsilon = 0$ again.

Figure 3 shows calculated conductance as a function of a magnetic field in the presence of a single impurity at an A site in armchair nanotubes for several $\tilde{u}$, where we set $L/\sqrt{3}a$=30. Solid and dashed lines show results obtained by an effective-mass theory and in a tight binding model, respectively, which show good agreement in all range of the magnetic field. In the case of a weak impurity potential $\tilde{u}$<1, the conductance decreases with the increase of the field and approaches the conductance quantum $e^2/\pi\hbar$ in the strong-field limit. In the case of a strong impurity potential $\tilde{u}\gg$1, the conductance is quantized into $e^2/\pi\hbar$ independent of the field. These results are in agreement with those obtained in CN with a single lattice-vacancy.[28]

Figure 4 shows calculated transmission and reflection probabilities in the presence of a single impurity potential at an A site in armchair nanotubes for $\tilde{u}$=1.0. In the weak-field regime, both intra- and inter-valley processes occur and this leads to scattering wave with typical $\sqrt{3} \times \sqrt{3}$ periodicity around the impurity. In the high magnetic field, inter-valley scattering is suppressed and intra-valley transmission for in-coming channel K and reflection for K' have an equal amplitude, i.e., $|t_{KK}|=|r_{K'K'}|=1$. Because of the peculiar wave functions in a high magnetic field, we have $|t_{K'K'}|=|r_{KK}|=1$, if an impurity is situated at B site instead of A or when $\theta_H=\pi$.

Figure 5 shows calculated conductance in the presence

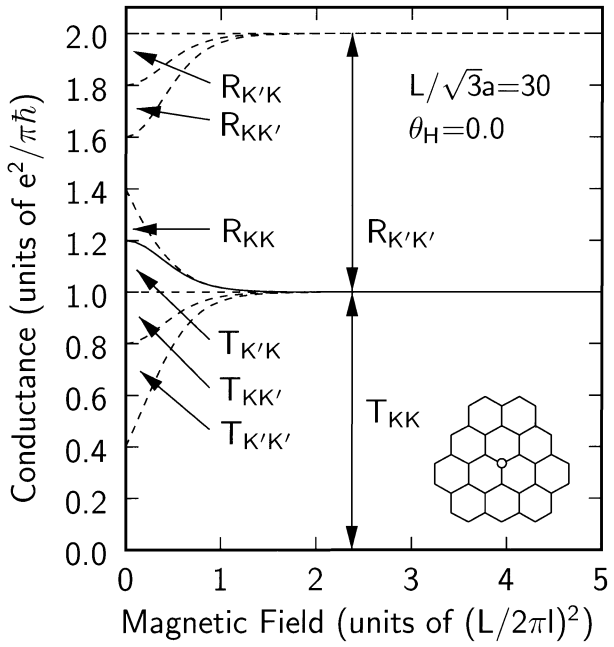

Fig. 4. Calculated transmission and reflection probabilities (dotted lines) and conductance (solid line) as a function of a magnetic field in the presence of a single impurity potential at an A site in armchair nanotubes for $\tilde{u}$=1.0.

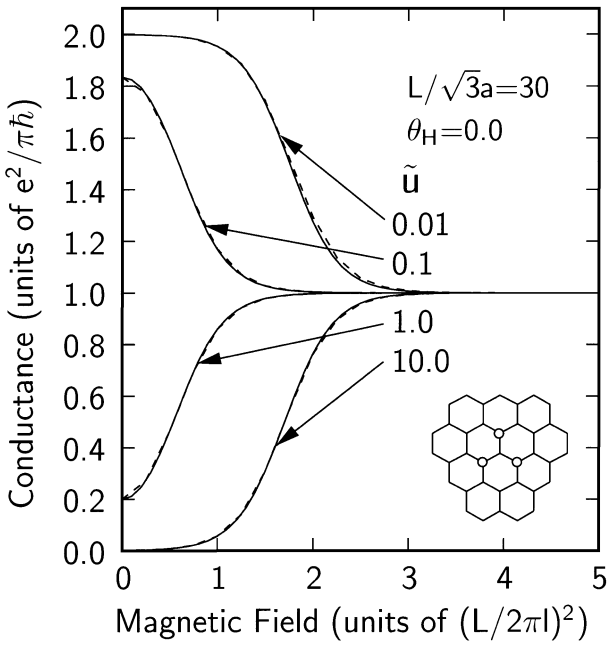

Fig. 5. Calculated conductance as a function of a magnetic field at ε=0 in the presence of A_3 impurities in armchair nanotubes for several $\tilde{u}$. $L/\sqrt{3}a$=30 and θ_H=0. Solid and dashed lines are results obtained by the effective-mass theory and in a tight-binding model, respectively.

of A_3 impurities in armchair nanotubes. In this case, the conductance is obtained by putting N=3 and M=3 in eq. (3.6). The conductance decreases with impurity potential and vanishes in the limit $\tilde{u}\gg1$ in the absence of a magnetic field. The field dependence is opposite between the case $\tilde{u}<1/3$ and $\tilde{u}>1/3$ and disappears when $\tilde{u}=1/3$. In the strong-field limit, the conductance is quantized into $e^2/\pi\hbar$ independent of $\tilde{u}$. The vanishing conductance in the limit $\tilde{u}\to\infty$ corresponds to the case of an A_3 lattice-vacancy.

Figure 6 shows calculated conductance in the presence of an AB pair impurity in armchair nanotubes with $L/\sqrt{3}a$=30. In the effective-mass theory we have to introduce a cutoff n_c, which is determined by the condition that the corresponding wave length $2\pi/k_c$ with $k_c = 2\pi n_c/L$ should be comparable to the lattice constant a. Therefore we have roughly $n_c \sim L/a$. In actual calculations the cutoff is chosen as $n_c = 26$. Because of the singularity of the off-diagonal Green's function, the conductance is almost equal to $G = 2e^2/\pi\hbar$ in the absence of a magnetic field. It decreases monotonically with the field and vanishes in the strong-field limit. Furthermore it does not depend on the strength of the impurity potential except near $\tilde{u}=\pm\Gamma_{AB}$ corresponding to a resonance.[27)]

Calculated transmission and reflection probabilities in the presence of an AB pair impurity in armchair nanotubes for $\tilde{u}$=1.0 are shown in Fig. 7. In the absence of a magnetic field, the back scattering within the same valley r_{KK} and $r_{K'K'}$ and the transmission between different valleys $t_{KK'}$ and $t_{K'K}$ are absent because of a mirror symmetry of impurities about a plane containing the axis.[18)] Inter-valley components in transmission and

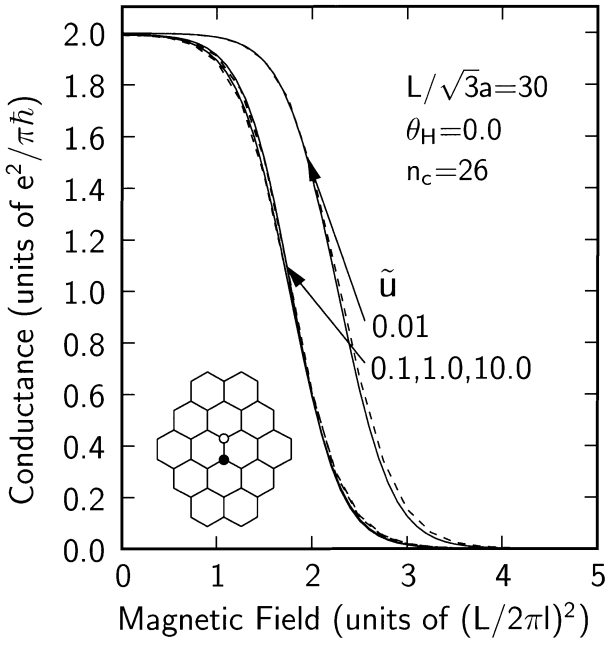

Fig. 6. Calculated conductance as a function of a magnetic field at $\varepsilon = 0$ in the presence of an AB pair impurity locates along a circumference direction in armchair nanotubes for several $\tilde{u}$. $L/\sqrt{3}a = 30$, $\theta_H = 0$ and $n_c = 26$. Solid and dashed lines are results obtained by the effective-mass theory and in a tight-binding model, respectively.

reflection coefficients gradually increase, reach maximum around $(L/2\pi l)^2 \sim 1.7$, and then decrease with the field. In strong-field, the conductance vanishes and the reflection occurs within the same valley.

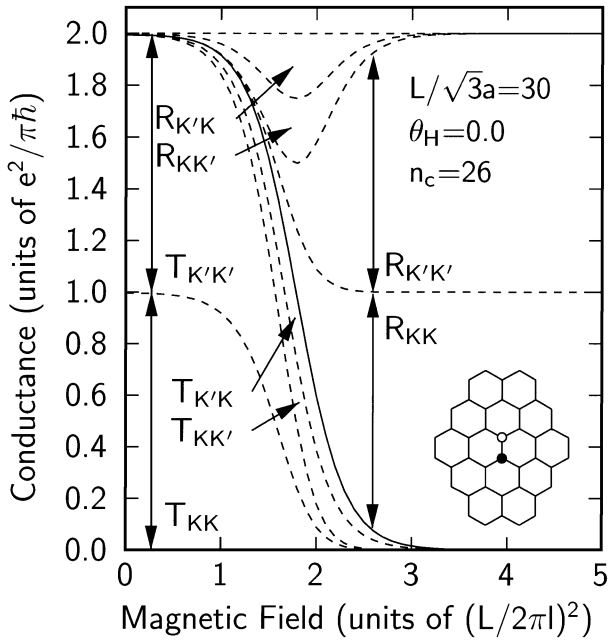

Fig. 7. Calculated transmission and reflection probabilities (dotted lines) and conductance (solid line) as a function of a magnetic field in the presence of an AB pair impurity locates along a circumference direction in armchair nanotubes for $\tilde{u}$=1.0.

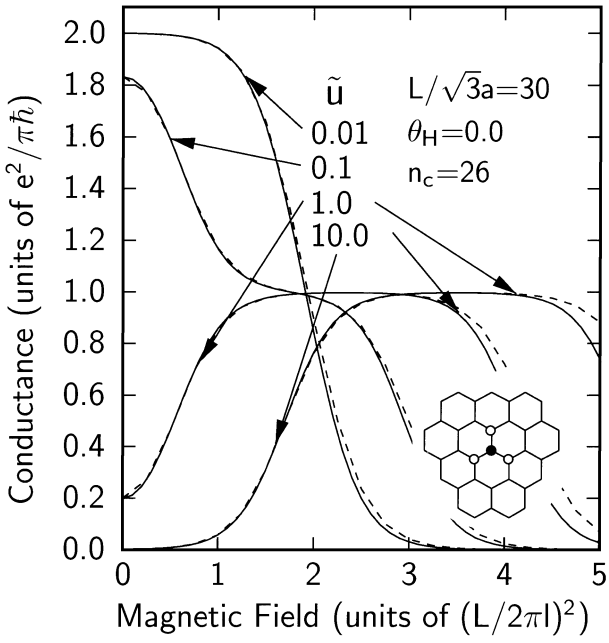

Fig. 8. Calculated conductance as a function of a magnetic field at $\varepsilon = 0$ in the presence of A_3B impurities in armchair nanotubes for several $\tilde{u}$. $L/\sqrt{3}a = 30$, $\theta_H = 0$ and $n_c = 26$. Solid and dashed lines are results obtained by the effective-mass theory and in a tight-binding model, respectively.

Figure 8 shows calculated conductance in the presence of AB_3 impurities in armchair nanotubes, where $L/\sqrt{3}a$=30 and $n_c = 26$. In the case of a weak impurity potential $\tilde{u}$<1, the conductance decreases with the increase of the field and approaches zero in the strong-field limit. In the case of a strong impurity potential $\tilde{u}$>1, we can neglect scattering from impurity at a B site because of the singularity of the off-diagonal Green's function in the weak-field limit. Consequently multiple scattering among A sites becomes dominant and the transmission probability of in-coming channel K increases with the field until $(L/2\pi l)^2 \sim 2$. The conductance takes nearly a quantized values $e^2/\pi\hbar$ in the intermediate field region. In the strong-field limit, we cannot ignore an impurity at a B site. Therefore, both in-coming channels K and K' are strongly scattered and the conductance vanishes.

Figure 9 shows calculated conductance for $A_{43}B_{42}$ impurities localized within a circle with a radius $w/a \simeq 6.0$ and a center at an atomic site. We have $L/\sqrt{3}a$=30 and $n_c = 26$. In the case of weak potential $\tilde{u}$=0.01, the conductance decreases with the increase of the field and vanishes in the strong-field limit as in the case of simpler examples. In the case of a strong impurity $\tilde{u} \geq 1$, on the other hand, the effective scattering from the $A_{43}B_{42}$ impurities is reduced to that of a single impurity at an A site because $\Delta N_{AB} = 1$. Further, the conductance remains at $e^2/\pi\hbar$ until $(L/2\pi l)^2$=2 ∼ 3 and vanishes in the strong-field limit. The conductance shows a sharp resonance around $\tilde{u} \simeq 0.01$ and the resonance position is quite sensitive to various parameters including n_c. This is the origin of a large deviation between the results in a tight-binding model and an effective-mass theory for $\tilde{u}$=0.01.

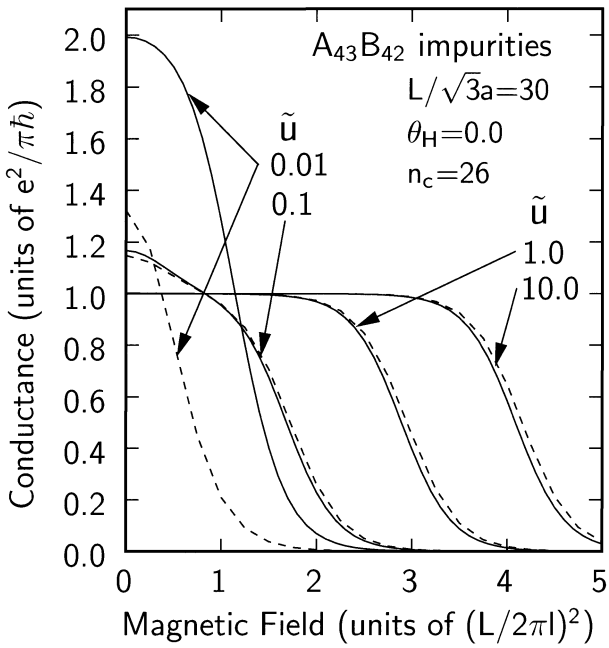

Fig. 9. Calculated conductance as a function of a magnetic field at $\varepsilon = 0$ in the presence of circular site-center $A_{43}B_{42}$ impurities in armchair nanotubes for several $\tilde{u}$. $L/\sqrt{3}a = 30$, $\theta_H = 0$ and $n_c = 26$. Solid and dashed lines are results obtained by the effective-mass theory and in a tight-binding model, respectively.

§5. Summary and Discussion

In this paper, we have studied effects of short-range impurities on transport of CN based on an effective-mass theory in the presence of a magnetic field perpendicular to the axis. The results are summarized as follows:

Green's functions describing propagation between same and different sublattices have different magnetic-field and distance dependence. The former is safely replaced by the local density of states at the center-of-mass of impurities $\boldsymbol{r}_0$ and depends only on the field component in the direction of the $\boldsymbol{r}_0$, i.e, $H\cos\theta_H$. On the other hand, the latter does not depend on the field and takes an extremely large value when impurities are localized within a distance of a few times of the lattice constant. As a result both T and S matrices are a function of $H\cos\theta_H$, leading to the conclusion that the conductance is also a function of $H\cos\theta_H$. This is the origin of the conductance scaling we found in the previous numerical study.[28)]

The conductance exhibits characteristic field variation depending critically on the number of impurities. This is closely related to relative importance of diagonal and off-diagonal Green's functions at the center-of-mass of impurities. In the weak-field regime, where the off-diagonal Green's function is much larger than the diagonal term, the conductance strongly depends on the strength of potential and difference ΔN_{AB} in the number of impurities at A and B sublattices. In the limit of strong scatterers, i.e., $\tilde{u}\geq 1$, the conductance is almost equal to ideal $2e^2/\pi\hbar$ in the absence of the field and vanishes monotonically with the field when $|\Delta N_{AB}|=0$. In the case $|\Delta N_{AB}|=1$, the conductance is reduced to a half of the ideal value and does not depend on the field in intermediate fields. In the case $|\Delta N_{AB}|\geq 2$, the conductance vanishes in the absence of a field but increases up to a half of the ideal value in intermediate fields.

In the strong-field limit, Landau wave functions for A and B sites are localized in a spatial region different from each other, i.e., around a bottom and a top of CN. Therefore, an overlap integral of envelope functions for the A and B site becomes smaller, and we can ignore contribution of the off-diagonal Green's functions and treat A and B sublattices separately. Consequently the conductance is quantized into $e^2/\pi\hbar$ if impurities exist in only A or B sites. In other cases, the conductance always becomes zero independent of ΔN_{AB}.

There have been some experimental efforts to synthesize CN with hetero atoms like boron and nitrogen. Electronic and geometric structures of B-doped multiwalled-CN's were studied with STS measurements and the formation of a nanodomain of BC_3 islands was suggested.[41)] In this system, a doped boron will act as a local impurity in the host CN.

Effects of a single B and N atom on transport in a (10,10)-armchair nanotube were studied using an *ab initio* pseudopotential method within a Landauer formalism.[42)] It was shown that doped B and N produce a quasi-bound impurity state at 0.70 eV below and 0.53 eV above the Fermi energy, respectively, and the conductance is given by $\sim e^2/\pi\hbar$ at the corresponding energy. The origin of this conductance is essentially same as that of a single impurity case which we have already discussed in ref. 27. In this case, the strength of the impurity potential is estimated as $V\sim -1.5$ and 2.2 eV for B and N, respectively, using eq. (2.77) of ref. 27 and eq. (4.1). This impurity strength is of the same order as that of the nearest-neighbor hopping integral γ_0. For a multi-wall nanotube with L/a=300, for example, we have $\tilde{u}$=1/600 in the case $V=\gamma_0$ and the magnetic field corresponding to $(L/2\pi l)^2$=1 and 5 is given by 4.9 and 24.7 T, respectively.

Another intriguing way to introduce local impurities is fluorination of the sp^2 carbon.[43,44)] Electronic and geometric structures of a fluorinated graphene sheet are being studied using an *ab initio* pseudopotential method.[45)] A doped fluorine makes a covalent bond with an sp^2 carbon and the charge density distribution shows a typical $\sqrt{3}\times\sqrt{3}$ structure near the Fermi level. This means that the doped fluorine acts as a local defect in π-electron network of a graphene sheet.

Acknowledgments

Two of the authors, M.I. and T.N., acknowledge the support of a research fellowship from the Japan Society for the Promotion of Science for Young Scientists. This work was supported in part by Grants-in-Aid for Scientific Research and for Priority Area, Fullerene Network, from the Ministry of Education, Science, Sports and Culture, Japan. Numerical calculations were performed in part at the Supercomputer Center, Institute for Solid State Physics, University of Tokyo and at the Supercomputer Center, Institute for Molecular Science.

1) S. Iijima: Nature (London) **354** (1991) 56.
2) N. Hamada, S. Sawada and A. Oshiyama: Phys. Rev. Lett. **68** (1992) 1579.
3) J. W. Mintmire, B. I. Dunlap and C. T. White: Phys. Rev. Lett. **68** (1992) 631.
4) R. Saito, M. Fujita, G. Dresselhaus and M. S. Dresselhaus: Phys. Rev. B**46** (1992) 1804; Appl. Phys. Lett. **60** (1992) 2204.
5) M. S. Dresselhaus, G. Dresselhaus and R. Saito: Phys. Rev. B **45** (1992) 6234.
6) R. A. Jishi, M. S. Dresselhaus and G. Dresselhaus: Phys. Rev. B **47** (1993) 16671.
7) K. Tanaka, K. Okahara, M. Okada and T. Yamabe: Chem. Phys. Lett. **191** (1992) 469.
8) Y. D. Gao and W. C. Herndon: Mol. Phys. **77** (1992) 585.
9) D. H. Robertson, D. W. Berenner and J. W. Mintmire: Phys. Rev. B **45** (1992) 12592.
10) C. T. White, D. C. Robertson and J. W. Mintmire: Phys. Rev. B **47** (1993) 5485.
11) H. Ajiki and T. Ando: J. Phys. Soc. Jpn. **62** (1993) 1255.
12) A. M. Rao, E. Richter, S. Bandow, B. Chase, P. C. Eklund, K. W. Williams, M. Menon, K. R. Subbaswamy, A. Thess, R. E. Smalley, G. Dresselhaus and M. S. Dresselhaus: Science **275** (1997) 187.
13) C. H. Olk and J. P. Heremans: J. Mater. Res. **9** (1994) 259.
14) J. W. G. Wildöer, L. C. Venema, A. G. Rinzlert, R. E. Smalley and C. Dekker: Nature (London) **391** (1998) 59.
15) A. Hassanien, M. Tokumoto, Y. Kumazawa, H. Kataura, Y. Maniwa, S. Suzuki and Y. Achiba: Appl. Phys. Lett. **73** (1998) 3839.
16) L. Chico, L. X. Benedict, S. G. Louie and M. L. Cohen: Phys. Rev. B **54** (1996) 2600.; Phys. Rev. B **61** (2000) 10511 (Erratum).
17) R. Tamura and M. Tsukada: Phys. Rev. B **55** (1997) 4991.
18) H. Matsumura and T. Ando: J. Phys. Soc. Jpn. **67** (1998) 3542.
19) T. Yaguchi, Master thesis (Univ. Tokyo, 2000).
20) M. Fujita, K. Wakabayashi, K. Nakada and K. Kusakabe: J. Phys. Soc. Jpn. **65** (1996) 1920.

21) K. Nakada, M. Fujita, G. Dresselhaus and M. S. Dresselhaus: Phys. Rev. B **54** (1996) 17954.
22) M. Fujita, M. Igami and K. Nakada: J. Phys. Soc. Jpn. **66** (1997) 1864.
23) H. A. Mizes and J. S. Foster: Science **244** (1989) 559.
24) T. Ando and T. Nakanishi: J. Phys. Soc. Jpn. **67** (1998) 1704.
25) T. Nakanishi and T. Ando: J. Phys. Soc. Jpn. **68** (1999) 561.
26) T. Ando, T. Nakanishi and R. Saito: J. Phys. Soc. Jpn. **67** (1998) 2857; Microelectronic Engineering **47** (1999) 421.
27) T. Ando, T. Nakanishi and M. Igami: J. Phys. Soc. Jpn. **68** (1999) 3994.
28) M. Igami, T. Nakanishi and T. Ando: J. Phys. Soc. Jpn. **68** (1999) 716.
29) M. Igami, T. Nakanishi and T. Ando: J. Phys. Soc. Jpn. **68** (1999) 3146.
30) M. Igami, T. Nakanishi and T. Ando: Mol. Cryst. Liq. Cryst. **340** (2000) 719.
31) T. Nakanishi, M. Igami and T. Ando: Physica. E **6** (2000) 872.
32) M. Igami, T. Nakanishi and T. Ando: Physica. B **284–288** (2000) 1746.
33) T. Ando: Semicond. Sci. & Technol. **15** (2000) R13.
34) H. Ajiki and T. Ando: J. Phys. Soc. Jpn. **62** (1993) 2470.
35) R. Saito, G. Dresselhaus and M. S. Dresselhaus: Phys. Rev. B **50** (1994) 14698; Phys. Rev. B **53** (1996) 10408 (Erratum).
36) H. Ajiki and T. Ando: J. Phys. Soc. Jpn. **65** (1996) 505.
37) T. Seri and T. Ando: J. Phys. Soc. Jpn. **66** (1997) 169.
38) T. Ando and T. Seri: J. Phys. Soc. Jpn. **66** (1997) 3558.
39) T. Nakanishi and T. Ando: J. Phys. Soc. Jpn. **66** (1997) 2973.
40) R. Landauer: IBM J. Res. Dev. **1** (1957) 223; Philos. Mag. **21** (1970) 863.
41) D. L. Carroll, Ph. Redlich, X. Blase, J.-C. Charlier, S. Curran, P. M. Ajayan, S. Roth and M. Rühle: Phys. Rev. Lett. **81** (1998) 2332.
42) H. J. Choi, J. Ihm, S. G. Louie and M. L. Cohen: Phys. Rev. Lett. **84** (2000) 2917.
43) K. Takai, H. Sato, T. Enoki, N. Yoshida, F. Okino, H. Touhara and M. Endo: Mol. Cryst. Liq. Cryst. **340** (2000) 289.
44) R. Saito, M. Yagi, T. Kimura, G. Dresselhaus and M. S. Dresselhaus: J. Phys. Chem. Solid **60** (1999) 715.
45) M. Igami, S. Okada and K. Nakada: (*in preparation*).